Cell Death & Differentiation (2021) 28:1579–1592
https://doi.org/10.1038/s41418-020-00687-7

Cell Death & Differentiation

ARTICLE

Antiapoptotic Bcl-2 family proteins BCL-xL and MCL-1 integrate neural progenitor survival and proliferation during postnatal cerebellar neurogenesis

Katherine A. Veleta[1] · Abigail H. Cleveland[2] · Benjamin R. Babcock[3] · You-Wen He[4] · Duhyeong Hwang[5] · Marina Sokolsky-Papkov[5] · Timothy R. Gershon[1,3,6]

Received: 12 September 2019 / Revised: 11 November 2020 / Accepted: 16 November 2020 / Published online: 8 December 2020

Abstract

The tendency of brain cells to undergo apoptosis in response to exogenous events varies across neural development, with apoptotic threshold dependent on proliferation state. Proliferative neural progenitors show a low threshold for apoptosis, while terminally differentiated neurons are relatively refractory. To define the mechanisms linking proliferation and apoptotic threshold, we examined the effect of conditionally deleting *Bcl2l1*, the gene that codes the antiapoptotic protein BCL-xL, in cerebellar granule neuron progenitors (CGNPs), and of co-deleting *Bcl2l1* homologs, antiapoptotic *Mcl-1*, or pro-apoptotic *Bax*. We found that cerebella in conditional *Bcl2l1*-deleted (*Bcl-xL*^{cKO}) mice were severely hypoplastic due to the increased apoptosis of CGNPs and their differentiated progeny, the cerebellar granule neurons (CGNs). Apoptosis was highest as *Bcl-xL*^{cKO} CGNPs exited the cell cycle to initiate differentiation, with proliferating *Bcl-xL*^{cKO} CGNPs relatively less affected. Despite the overall reduction in cerebellar growth, SHH-dependent proliferation was prolonged in *Bcl-xL*^{cKO} mice, as more CGNPs remained proliferative in the second postnatal week. Co-deletion of *Bax* rescued the *Bcl-xL*^{cKO} phenotype, while co-deletion of *Mcl-1* enhanced the phenotype. These findings show that CGNPs require BCL-xL to regulate BAX-dependent apoptosis, and that this role can be partially compensated by MCL-1. Our data further show that BCL-xL expression regulates MCL-1 abundance in CGNPs, and suggest that excessive MCL-1 in *Bcl-xL*^{cKO} mice prolongs CGNP proliferation by binding SUFU, resulting in increased SHH pathway activation. Accordingly, we propose that BCL-xL and MCL-1 interact with each other and with developmental mechanisms that regulate proliferation, to adjust the apoptotic threshold as CGNPs progress through postnatal neurogenesis to CGNs.

Introduction

In the developing nervous system, the apoptotic decisions of individual cells have risks and benefits to the organism that vary with proliferative state. Early in development, the apoptosis of DNA-damaged progenitors can be advantageous in preventing the propagation of mutations. Excessive apoptosis of dividing progenitors, however, can inappropriately limit growth by ablating the potential progeny of

These authors contributed equally: Katherine A. Veleta, Abigail H. Cleveland

Edited by R. Kitsis

Supplementary information The online version of this article (https://doi.org/10.1038/s41418-020-00687-7) contains supplementary material, which is available to authorized users.

✉ Timothy R. Gershon
gershont@neurology.med.unc.edu

[1] UNC Neuroscience Center, University of North Carolina, Chapel Hill, NC 27599, USA

[2] UNC Cancer Cell Biology Training Program, University of North Carolina, Chapel Hill, NC 27599, USA

[3] Department of Neurology, UNC School of Medicine, University of North Carolina, Chapel Hill, NC 27599, USA

[4] Department of Immunology, Duke University, Durham, NC 27708, USA

[5] Center for Nanotechnology in Drug Delivery and Division of Pharmacoengineering and Molecular Pharmaceutics, Eshelman School of Pharmacy, University of North Carolina at Chapel Hill, Chapel Hill, NC 27599, USA

[6] Lineberger Comprehensive Cancer Center, University of North Carolina, Chapel Hill, NC 27599, USA

the dividing cell. The risks of apoptosis change as progenitor self-renewal decreases. Progenitors with limited self-renewal have fewer progeny, reducing the risk that their apoptosis will impair growth. Later in development, when progenitors have exited the cell cycle and differentiated into neurons, the implications of apoptotic decisions are again different. If mature neurons sustain DNA damage, there is no risk of propagating mutations, but the cell cannot be replaced through proliferation if it undergoes apoptosis. We propose that these different risks and benefits shape the mechanisms that regulate apoptosis in early progenitors, late progenitors, and neurons, and that these mechanisms can be elucidated in the developmental progression of cerebellar granule neuron progenitors (CGNPs) to cerebellar granule neuron (CGNs).

CGNPs proliferate in the external granule layer (EGL) of the cerebellum, during the first 15 days of life in mice, and the first year of life in humans, in response to locally secreted Sonic Hedgehog (SHH). In mice, CGNP proliferation wanes from P7-15, as individual CGNPs exit the cell cycle, moving from the proliferative outer EGL (oEGL), distinguished by proliferation markers PCNA and phosphorylated RB (pRB), to the differentiating inner EGL (iEGL). Differentiating CGNPs then migrate to the internal granule layer (IGL) to become terminally differentiated CGNs [1–3].

We have shown that CGNPs are primed for apoptosis by maintaining pro-apoptotic BAX in an active conformation [4]. Most cell types maintain BAX in its inactive conformation unless apoptosis is initiated. However, CGNPs, like other proliferative cell types, maintain a state of apoptotic priming in which BAX is kept in its active conformation, bound to antiapoptotic proteins to prevent spontaneous apoptosis [5–8]. Apoptotic priming reduces the threshold stimulus required to trigger cell death. Consistent with apoptotic priming, we showed that CGNPs harbor active BAX complexed with BCL-xL, and that pro-apoptotic stimulus disrupted the BCL-xL:BAX interaction [4]. These findings suggest that CGNPs use BCL-xL to prevent inappropriate triggering of apoptosis, but do not resolve how CGNPs regulate apoptotic threshold over the course of neuronal differentiation.

Prior studies have shown BCL-xL dependence increases with differentiation. Conditional deletion of *Bcl2l1*, the locus that encodes *Bcl-xL*, causes neurons throughout the central nervous system, including retinal ganglion cells and neurons of the cerebral cortex and spinal cord, to undergo apoptosis after differentiating from progenitors [9–12]. These studies of different CNS regions show a consistent pattern in which BCL-xL is required for neuronal survival. However, the role of BCL-xL in progenitors is unclear, and remains complicated by divergent requirements for the BCL-xL homolog MCL-1 in different experimental contexts.

Conditional deletion studies of *Mcl-1* in the nervous system have produced conflicting results on progenitor dependence. Studies using one conditional mouse line showed marked phenotypes caused by *Mcl-1* deletion, with apoptosis of embryonic and adult neural progenitors [12–14]. However, we found that conditional deletion of *Mcl-1* in cerebellar progenitors, using an independently generated conditional mouse line, did not induce CGNP apoptosis and produced no detectable phenotype [4]. Both *Mcl-1* conditional deletion lines similarly harbor loxP sites surrounding the first exon, and the reason for the divergence in phenotypes is not clear.

We investigated the developmental dynamics of apoptosis regulation in the CNS by conditionally deleting *Bcl2l1* in the CGNP lineage, either alone or in combination with either *Mcl-1* or *Bax*. Our data show an interrelation between antiapoptotic proteins that changes over the course of postnatal cerebellar neurogenesis, affects mitogenic signaling and differs from prior findings in cerebral development.

Materials and methods

Mice

We generated *Bcl-xL*^{cKO} mice by crossing *Math1-Cre* (Jackson Labs, stock #011104) and *Bcl2l1* $^{LoxP/LoxP}$ [15] mouse lines. To generate the *Bcl-xL/Bax*^{dKO}, *Bax* $^{LoxP/LoxP}$ mice were acquired as Bax $^{LoxP/LoxP}$;Bak$^{-/-}$ from Jackson Laboratories and selectively bred to replace both mutant Bak alleles with wild-type alleles. Co-deletion of *Bcl2* and *Bax* was then accomplished by crossing *Bax* $^{LoxP/LoxP}$ mice into the *Bcl-xL*^{cKO} line. To generate mice with *Bcl-xL* and *Mcl-1* co-deletion (*Bcl-xL/Mcl-1*^{cKO}) we bred *Mcl-1*$^{LoxP/LoxP}$ animals [16] with the *Bcl-xL*^{cKO} line. All experiments were conducted in accordance with the approval and guidelines of the University of North Carolina at Chapel Hill's Institutional Animal Care and Use Committee (IACUC#13-121,16-099, 18-107). All mice for these experiments were of the species *Mus musculus*, maintained on the C57/BLK6 background. The number of replicates in each experiment is specified in the figure legend and graphed as individual data points. All replicates represent individual mice and are thus biological replicates. Sample sizes were based on sample sizes adequate in prior published studies [4, 17, 18]. Genotypes were determined by PCR and the presence or absence of BCL-xL protein was verified by immunohistochemistry. Mice of each genotype were randomly selected to include both males and females at postnatal days 7, 12, 16, and 20. Blinding could not be achieved due to the overt symptoms of the *Bcl-xL*^{cKO} phenotype.

Histology and Immunohistochemistry of cerebellar sections

Mouse brain specimens were processed, sectioned and stained as previously described [17, 18] using primary antibodies: BCL-xL diluted 1:300 (Cell Signaling, #2764), pRB diluted 1:3000 (Cell Signaling, #8516), phosphorylated histone H3 (pHH3) diluted 1:100 (Cell Signaling, #9706), cleaved caspase-3 (cC3) diluted 1:50 (Cell Signaling, #9664), PCNA diluted 1:2000 (Cell Signaling, #2586), MATH1 (Aka ATOH-1) diluted 1:200 (Abcam, #ab105497), and CyclinD1 (CCND1) diluted 1:500 (Cell Signaling, #2978). For immunofluorescence (IF), nuclei were counterstained with 4′6-diamino-2-phenylindole (DAPI; Thermo Fisher Scientific, #D1306), 200 ng/mL, for 20 min and immunoreactivity was evaluated with a Leica epifluorescence DM5000B microscope (Leica Microsystems). Stained slides were digitally acquired using an Aperio ScanScope XT (Aperio). For quantification, the EGL, IGL, and whole cerebella were manually annotated on each section then subjected to automated cell counting using Tissue Studio (Definiens).

CGNP isolation and flow cytometry

CGNPs were isolated at P7 from WT or *Bcl-xL*^{cKO} mice as previously described [17] In brief, whole cerebella were dissected free of meninges, then dissociated in papain at 37 °C for 15 min and selected on a density gradient of ovomucoid inhibitor (Worthington Biochemical Corporation, #LK003150). Dissociated CGNPs were fixed, permeabilized and then stained. CGNPs were stained for DNA content using FxCycle Violet at 1:100 (Life Technologies, #F10347), for proliferation with 647-conjugated pRB antibodies diluted 1:50 (Cell Signaling, #89745) and for MCL-1 expression with PE-conjugated MCL-1 antibodies diluted 1:50 (Cell Signaling, #65617). Cells were then analyzed using an LSRFortessa (BD Biosciences) at the UNC Flow Cytometry Core Facility. Flow cytometry data generated were analyzed using FlowJo v10 (FloJO, Becton Dickinson).

Immunoprecipitation

CGNPs were dissociated as above and centrifuged at 1000 rpm for 10 min at 4 °C. Cells were resuspended in CHAPS lysis buffer containing protease inhibitors and placed on a rocker at 4 °C for 10 min, followed by 20 min on ice. Lysates were spun down at 13,300 rpm for 30 min at 4 °C and resulting supernatants were used for immunoprecipitation. Immunoprecipitations (IP) were performed by incubating 100 µg of protein from each sample with 40 µL of either MCL-1 antibody-Agarose conjugate (Santa Cruz, sc-12756) or control mouse IgG-Agarose conjugate (Santa Cruz, sc-2343), and diluted to a total volume of 300 µL with CHAPS buffer. Samples were rocked at 4 °C for 2 h. After extensive washing with CHAPS buffer, beads were boiled in 30 µL of an LDS Sample Buffer (Thermo Fisher Scientific, B0008) and DTT (Thermo Fisher Scientific, NXA32001) solution, and 20 µL of the eluted proteins were analyzed by western blot as described below. Western blot analysis of pre-IP (labeled Input) and immunoprecipitated samples (labeled IP) were also performed as described below using a 7.5:5000 concentration for secondary antibodies.

Western blot

For western blot whole cerebella were homogenized in lysis buffer (Cell Signaling, #9803), except in IP experiments as described above. Protein concentrations were quantified using the Pierce™ BCA Protein Assay Kit (Thermo Fisher Scientific, #23225) and equal concentrations of protein were resolved on SDS-polyacrylamide gels then transferred to polyvinylidene difluoride membranes. Immunologic analysis was performed on a SNAP ID device (Millipore) using manufacturer's protocol. Primary antibodies were: from Cell Signaling, β-Actin (1:5000, #4970), MCL-1 (1:500, #94296), BCL-xL (1:500, #2764), SUFU (1:500, #2522), BCL-2 (1:500, #3498) PUMA (1:500, #14570), BIM (1:500, #2933) and from Abcam, CDKN1A aka p21 (1:500, # ab109199). Secondary antibodies were Cell Signaling anti-rabbit IgG HRP (1:200, #7074), and anti-mouse IgG HRP (1:200, #7076). Western blots were developed using the enhanced chemiluminescent SuperSignal West Femto Maximum Sensitivity Substrate (Thermo Fisher Scientific, #34095) digitized using the C-DiGit blot scanner (LI-COR), and quantification was performed using Image Studio Lite software (LI-COR). The western blot was repeated twice with similar results.

POx-Vismo formulation

The amphiphilic triblock copolymer poly(Methyl-Butyl-Methyl) oxazoline (POx), P(MeOx37-b-BuOx21-b-MeOx36), was synthesized as previously described [19]. Vismodegib-loaded polyoxazoline micelles (POx-Vismo) were prepared using the thin-film hydration method as previously described [20, 21]. Briefly, vismodegib was mixed with POx solution in acetone, the acetone was evaporated and the resulting thin film was rehydrated with saline, allowing micelles to self-form. Samples were cooled to room temperature and centrifuged at 10k RPM for 3 min to remove any nonloaded Vismodegib. Micelle hydrodynamic diameter was determined by dynamic light scattering using a

Malvern Nanosizer (Malvern Instruments Ltd). Final POx-Vismo concentration was 100 µg/mL, determined by HPLC.

Vismodegib in vivo administration

For in vivo studies, *Bcl-xL*^{cKO} and control mice were injected IP with 100 mg/kg of POx-Vismodegib or an equal volume of saline control. Animals were injected at 24-h intervals for 2 consecutive days starting at P5 or P10. 24 h after the last injection, animals were sacrificed and brains were harvested for IHC or flow cytometry.

Results

Bcl-xL deletion in CGNPs reduces cerebellar growth while prolonging progenitor proliferation

Our prior finding that CGNPs maintain the pro-apoptotic protein BAX in its activated conformation suggested that these cells would require an antiapoptotic mechanism to prevent spontaneous apoptosis [4]. To determine if CGNPs depended on BCL-xL, we conditionally deleted *Bcl2l1* in the ATOH-1 (aka MATH1) lineage. ATOH-1 is a transcription factor expressed in a rostro-caudal pattern by CGNPs beginning at embryonic day 12.5 (E12.5) [22–24]. We bred *Math1-Cre* and *Bcl2l1* $^{loxP/loxP}$ mice [15] to generate *Math1-Cre/Bcl2l1*$^{loxP/loxP}$ (*Bcl-xL*^{cKO}) animals. We then compared *Bcl-xL*^{cKO} mice to littermate controls, including *Math1-Cre/Bcl2l1*$^{loxP/+}$ (*Bcl-xL*^{HET}) mice with heterozygous *Bcl2l1* deletion and mice without Cre, in which both alleles of *Bcl2l1* remained intact.

We found that *Bcl2l1* deletion caused severe, symptomatic cerebellar hypoplasia. *Bcl-xL*^{cKO} mice were viable and fertile, but exhibited ataxia by P12 and delayed ambulation, demonstrated by longer time spent in the center of an open field, compared to *Bcl-xL*-intact controls (Supplementary Fig. 1). The cerebella of *Bcl-xL*^{cKO} mice showed normal anatomy up to P7 (Fig. 1A). However, after P7 cerebellar growth decreased, and by P12 *Bcl-xL*^{cKO} cerebella were notably smaller than controls, with marked thinning of the CGNs of the IGL (Fig. 1A). Reduced cerebellar size and thinning of the IGL population became more pronounced by P20 (Fig. 1A).

We noted that the 2–4 most posterior-inferior lobules of the cerebella were relatively preserved in *Bcl-xL*^{cKO} cerebella (Fig. 1A). Math1-cre has been shown to delete target genes less efficiently in this region [25]. To determine if inefficient deletion of *Bcl2l1* accounted for the preservation of the posterior-inferior region, we compared BCL-xL protein distribution in P7 *Bcl-xL*^{cKO} and control cerebella. We found that BCL-xL protein was uniformly absent in the EGL of *Bcl-xL*^{cKO} mice, except in the most posterior-inferior lobules, where BCL-xL+ and BCL-xL- cells were intermixed in a mosaic pattern. In contrast, BCL-xL was uniformly present throughout the cerebellum in controls, including the entire EGL (Fig. 1B). Because *Bcl2l1* was mosaically deleted in the posterior-inferior region, we focused on anterior-superior lobules of the cerebellum in which BCL-xL was consistently ablated.

In light of the overall reduction in cerebellar growth, we were surprised to find that the proliferative CGNP population was increased at P12 in *Bcl-xL*^{cKO} cerebella. We noted that the EGL was abnormally thick in P12 *Bcl-xL*^{cKO} mice, compared to P12 controls, in which the EGL is expected to have thinned from its peak thickness at P7 (Fig. 1A). The thickened EGL in P12 *Bcl-xL*^{cKO} cerebella showed increased fractions of CGNPs expressing the proliferation marker pRB and the mitotic marker pHH3 (Fig. 1C,D).

To determine if cell cycle regulation was disrupted in the *Bcl-xL*^{cKO} cerebella, we analyzed the typically reciprocal patterns of expression of the proliferation marker PCNA and the cell cycle regulator CDKN2A (aka p27). In the WT cerebellum, proliferative CGNPs express PCNA in an outer layer within the EGL, while differentiating CGNPs express CDKN2A in a thin closely apposed layer of the EGL, and in the IGL. The *Bcl-xL*^{cKO} cerebella showed the expected PCNA+ and CDKN2A+ layers at both P7 and P12 (Fig. 1E), indicating that the orderly progression from proliferation, to cell cycle exit and differentiation was intact, but delayed. Moreover, studies of the p53-target CDKN1A (aka p21) showed no large change in p53-dependent gene expression (Supplementary Fig. 2). From these data, we conclude that the coordination of cell cycle regulators was not disrupted by *Bcl2l1* deletion. Thus, the *Bcl-xL*^{cKO} phenotype included two key features: reduced population of CGNs of the IGL and prolonged, regulated CGNP proliferation in the EGL.

BAX-dependent CGNP apoptosis drives growth failure in *Bcl-xL*^{cKO} cerebella

To determine if cerebellar hypoplasia in *Bcl-xL*^{cKO} mice resulted from increased apoptosis, we compared the apoptotic rate in *Bcl-xL*^{cKO} and control mice and determined whether *Bax* co-deletion rescued cerebellar growth. At P7, *Bcl-xL*^{cKO} cerebella showed increased fractions of cells expressing the apoptosis marker cleaved caspase-3 (cC3) compared to controls; apoptosis was increased in both the undifferentiated CGNPs of the EGL and the differentiated CGNs of the IGL (Fig. 2A, B).

To determine the contribution of BAX to this increased apoptosis, we co-deleted *Bcl2l1* and *Bax* by breeding *Bcl-xL*^{cKO} and Bax $^{loxP/loxP}$ lines to generate *Math1-Cre/Bcl2l1*$^{loxP/loxP}$/*Bax*$^{loxP/loxP}$ (*Bcl-xL/Bax*^{dKO}) mice. *Bcl-xL/Bax*^{dKO} mice were viable and fertile and unlike the *Bcl-xL*^{cKO}, did not develop

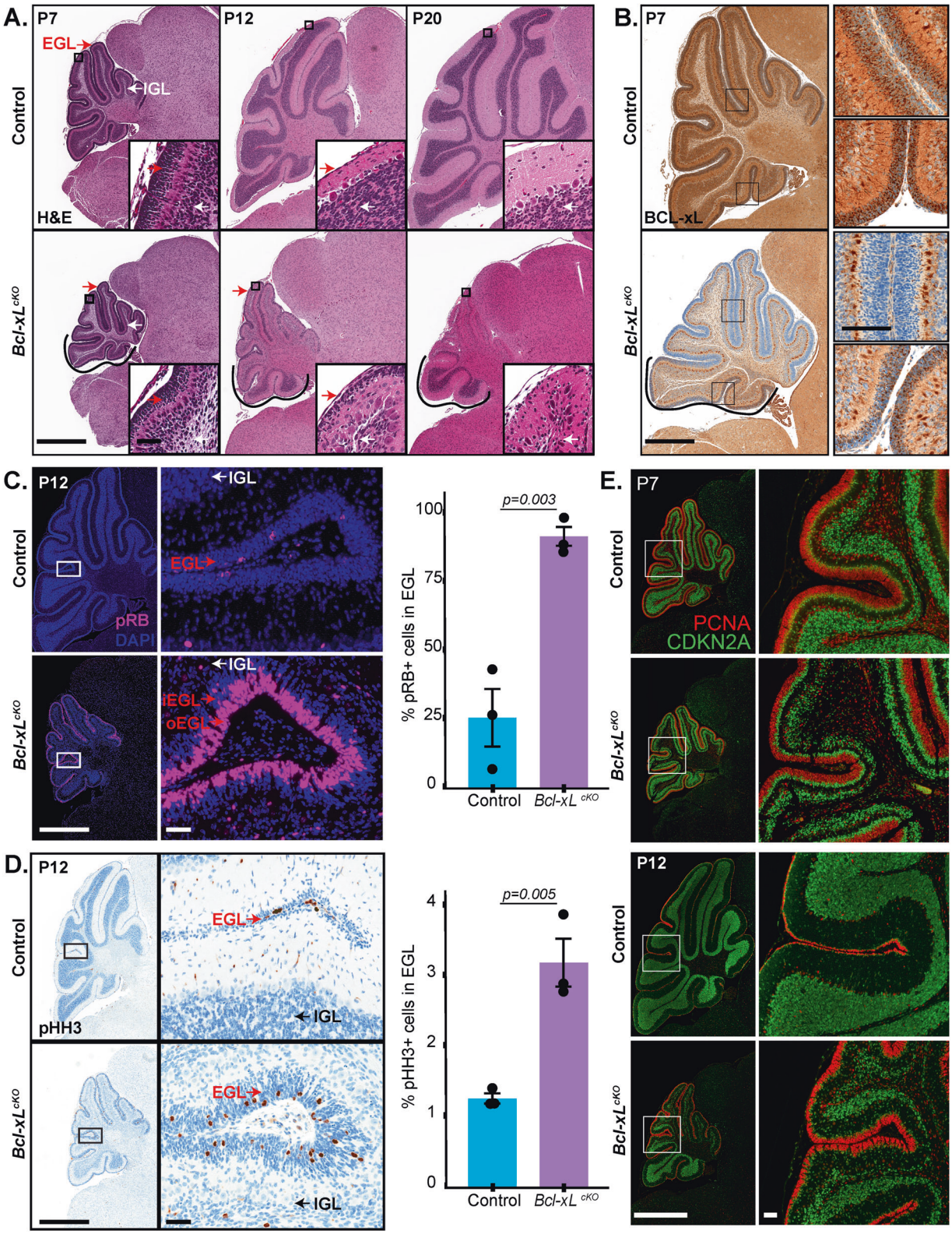

ataxia. The frequency of apoptosis in P7 *Bcl-xL/Bax*^{dKO} EGL and IGL was similar to WT controls (Fig. 2A, B). Cerebellar anatomy and development were normal in *Bcl-xL/Bax*^{dKO} mice (Fig. 2C) and the *Bcl-xL/Bax*^{dKO} mice showed no ataxia (Supplementary Fig. 1). The rescue of increased apoptosis at P7, cerebellar hypoplasia, and cerebellar function in *Bcl-xL/*

◀ **Fig. 1 *Bcl-xL^{cKO}* mice show cerebellar hypoplasia and prolonged CGNP proliferation in the EGL. A** Growth failure in *Bcl-xL^{cKO}* mice shown in representative H&E-stained sagittal brain sections from the indicated age and genotype. **B** IHC for BCL-xL in representative sagittal cerebellar sections from the indicated genotype, counterstained blue with hematoxylin, demonstrate absence of BCL-xL protein in *Bcl-xL^{cKO}* mice. **C** Representative pRB IF in sagittal cerebellar sections from P12 *Bcl-xL^{cKO}* and control mice, with the quantification of %pRB^{+} cells in the EGL from indicated genotypes, demonstrate increased EGL thickness and pRB expression in *Bcl-xL^{cKO}* cerebella. **D** Representative pHH3 IHC in sagittal cerebellar sections from P12 *Bcl-xL^{cKO}* and control mice, with the quantification of %pRB^{+} cells in the EGL from indicated genotypes, demonstrate increased mitoses in *Bcl-xL^{cKO}* cerebella. Arrows indicate the IGL, EGL, oEGL, and iEGL regions. **E** IHC for PCNA and CDKN2A in representative sections of the indicated age and genotype, demonstrate expected layering of proliferating and differentiating CGNPs in the *Bcl-xL^{cKO}* and control mice. Black curved line in **A**, **B** indicates the posterior-inferior folia that are preserved in the *Bcl-xL^{cKO}* mice. Size markers indicate 1 mm in low magnification images and 50 µm in high magnification images. Nuclei are counterstained with hematoxylin in IHC images and with DAPI in IF images. *P* values determined by two-tailed Student's *t*-test.

Bax^{dKO} mice establish BAX-dependent apoptosis as the primary cause of growth failure in the *Bcl-xL^{cKO}* phenotype.

Apoptosis remained increased in *Bcl-xL^{cKO}* cerebella at P12, and this increase was reduced, but not fully normalized in *Bcl-xL/Bax^{dKO}* mice (Fig. 2D, E). The increased proliferation noted in the EGL in P12 *Bcl-xL^{cKO}* mice was not observed in *Bcl-xL/Bax^{dKO}* mice (Fig. 2F, G). *Bax* co-deletion thus rescued both the cerebellar hypoplasia and the prolonged CGNP proliferation of the *Bcl-xL^{cKO}* phenotype, demonstrating that BCL-xL acts in CGNPs predominantly through its interaction with BAX. However, the statistically significant increase in CGNP apoptosis in the P12 *Bcl-xL/Bax^{dKO}* cerebella shows that BAX was the predominant, but not the only death regulator that is modulated by BCL-xL. Our prior finding that the BAX homolog BAK can drive apoptosis in *Bax*-deleted CGNPs, suggests that BAK may drive the residual cell death in the P12 cerebella.

Apoptosis in *Bcl-xL^{cKO}* CGNPs increases with cell cycle exit

CGNPs progress through proliferative and post proliferative, undifferentiated stages, which made it possible for us to examine the effects of cell cycle exit on BCL-xL dependence, prior to completion of neuronal differentiation. While the increased cell death in the *Bcl-xL^{cKO}* IGL showed BCL-xL dependence in early differentiated neurons, consistent with prior reports [9–11]; comparison of the oEGL and iEGL allowed us to specifically determine a link between BCL-xL-dependence and postproliferative state. To analyze cell death in the oEGL and iEGL, we compared the co-expression of cC3 and PCNA in *Bcl-xL^{cKO}*, *Bcl-xL/Bax^{dKO}*, and control cerebella at P7. We found increased apoptosis in *Bcl-xL^{cKO}* CGNPs in both the PCNA^{+} oEGL and the PCNA^{-} iEGL (Fig. 3A, B), demonstrating that CGNPs depend on BCL-xL before and after cell cycle exit. In controls, apoptosis was more frequent in proliferating CGNPs, such that the log ratio of apoptotic cells in PCNA^{-}:PCNA^{+} layers was negative, however, in the *Bcl-xL^{cKO}* mice, this relationship was reversed, with apoptosis higher in the PCNA^{-} population (Fig. 3C). Conversely, we noted in flow cytometry studies that at P7 the pRB^{+} fraction of CGNPs was larger in the *Bcl-xL^{cKO}* cerebella (Fig. 3D, E), consistent with selective removal of differentiating cells from the CGNP population.

Interaction between BCL-xL function and differentiation

To test experimentally whether BCL-xL dependence was causally linked to differentiation, we examined the effect of accelerating CGNP cell cycle exit by administering the SHH pathway inhibitor vismodegib to *Bcl-xL^{cKO}* and control mice. Vismodegib blocks SHH signaling by inhibiting the SHH receptor component SMO [26, 27]. To facilitate vismodegib administration, we used the recently developed nanoparticle formulation (POx-vismo) [28]. In both *Bcl-xL^{cKO}* mice and controls, daily administration of vismodegib over a 2-day period from P5-7 significantly increased cell cycle exit, demonstrated by reduced fractions of PCNA^{+} cells at P7 (Fig. 3F, G). Importantly, vismodegib depleted the EGL population significantly more in *Bcl-xL^{cKO}* mice than in controls, showing greater effect on both total cell density and density of PCNA^{+} cells (Fig. 3H, I). The greater reduction of the EGL by vismodegib in *Bcl-xL^{cKO}* mice is consistent with the induced differentiation in the absence of BCL-xL increasing cell death. It is also possible that *Bcl2l1* deletion may potentiate induction of differentiation by vismodegib, and that both processes may act in concert. In either case, the data show that BCL-xL function remains linked to CGNP cell cycle exit when cell cycle exit is accelerated.

CGNPs express MCL-1 during proliferation

To identify a mechanism for reduced BCL-xL dependence during proliferation, we analyzed the expression of the BCL-xL homolog, MCL-1 in WT CGNPs at different phases of the cell cycle. We found that MCL-1 expression in CGNPs varied across the cell cycle. CGNPs at G_0/G_1 showed a range of MCL-1 expression from detectable to undetectable, while CGNPs at S-G_2/M were consistently MCL-1^{+}, demonstrating both a higher fraction above threshold and a higher median fluorescence intensity (Fig. 4A, B). This proliferation-specific expression pattern identified MCL-1 as a potential mechanism that could

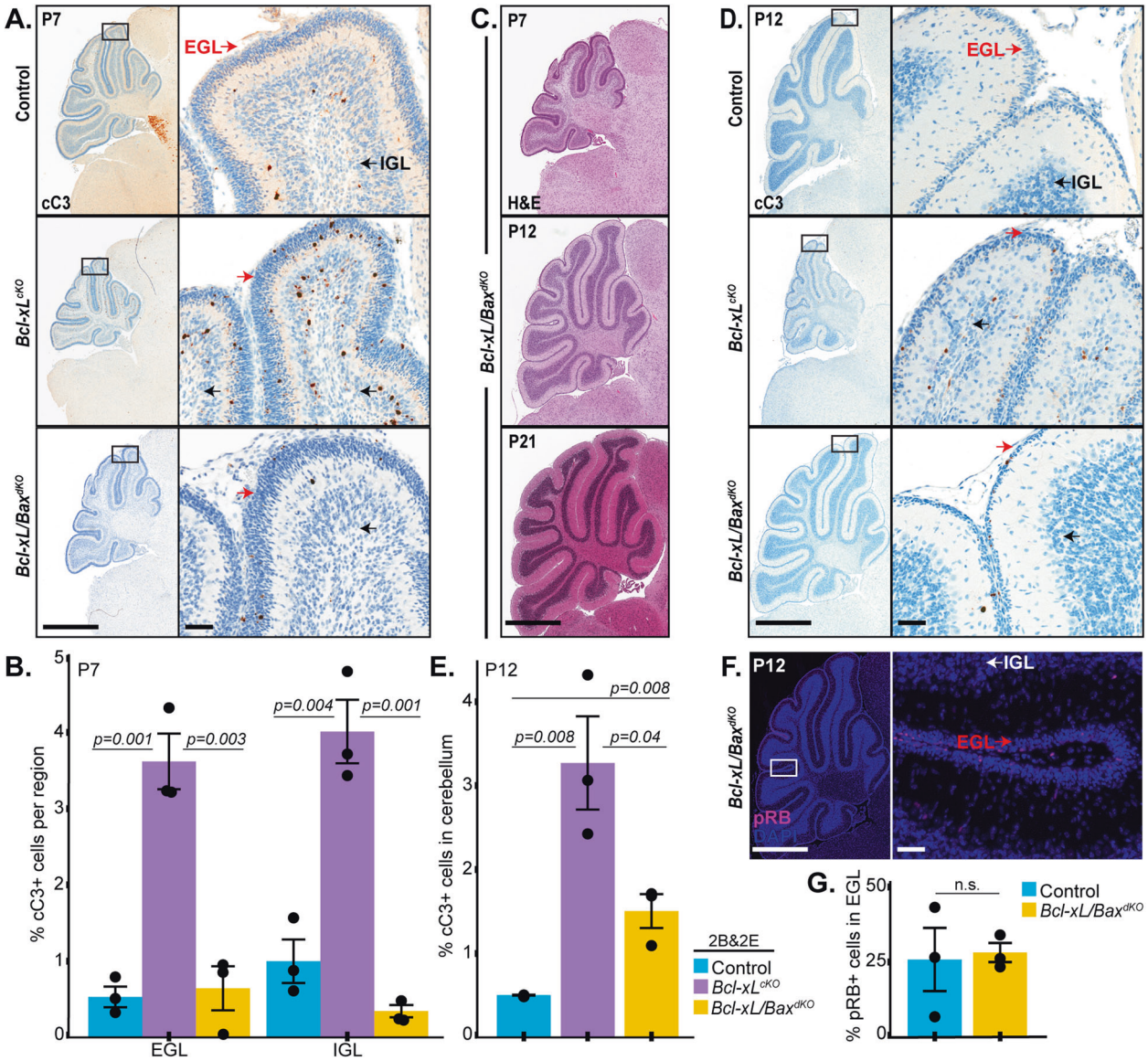

Fig. 2 Increased apoptosis in *Bcl-xL*^{cKO} mice is rescued by co-deletion of *Bax*. **A**, **B** Representative cC3 IHC in sagittal cerebellar sections from P7 *Bcl-xL*^{cKO}, *Bcl-xL;Bax*^{dKO}, and control mice, with the quantification of %cC3^{+} cells in the EGL and IGL from indicated genotypes, demonstrate increased apoptosis at P7 in *Bcl-xL*-deleted cerebella that is rescued by *Bax* co-deletion. **C** Normal cerebellar development in representative H&E sections of *Bcl-xL;Bax*^{dKO} cerebella at the indicated ages. **D**, **E** Representative IHC for cC3 in sagittal cerebellar sections from P12 *Bcl-xL*^{cKO}, *Bcl-xL;Bax*^{dKO}, and control mice, with the quantification of %cC3^{+} cells in the whole cerebella from indicated genotypes demonstrate increased apoptosis at P12 in *Bcl-xL*-deleted cerebella and that is significantly reduced, but not normalized, by *Bax* co-deletion. **F**, **G** Representative pRB IF images of sagittal cerebellar sections at P12 from *Bcl-xL/Bax*^{dKO} mice, with the quantification of %pRB^{+} cells in the EGL from indicated genotypes, shows that *Bax* co-deletion normalizes CGNP proliferation at P12. Control mice from figure 1D are presented in **G** for comparison. Arrows indicate the EGL and IGL regions. Size markers indicate 1 mm in low magnification images and 50 µm in high magnification images. Nuclei are counterstained with hematoxylin in IHC images and with DAPI in IF images. *P* values determined by two-tailed Student's *t*-test.

compensate for the loss of BCL-xL in *Bcl-xL*^{cKO} CGNPs during their proliferation.

BCL-xL depletion in *Bcl-xL*^{cKO} CGNPs increases MCL-1 protein abundance

We noted in flow cytometry studies that MCL-1 staining was markedly more intense in CGNPs from *Bcl-xL*^{cKO} mice compared to CGNPs from *Bcl-xL*-intact controls, indicating that individual *Bcl-xL*^{cKO} CGNPs contained more MCL-1 protein (Fig. 4C, D). Western blot studies confirmed increased MCL-1 abundance in *Bcl-xL*^{cKO} cerebellar lysates (Fig. 4E, F). Increased MCL-1 is likely to be mediated by increased MCL-1 stability, as MCL-1 abundance is known to be regulated by posttranslational degradation [29–31]. The increased MCL-1 in *Bcl-xL*^{cKO}

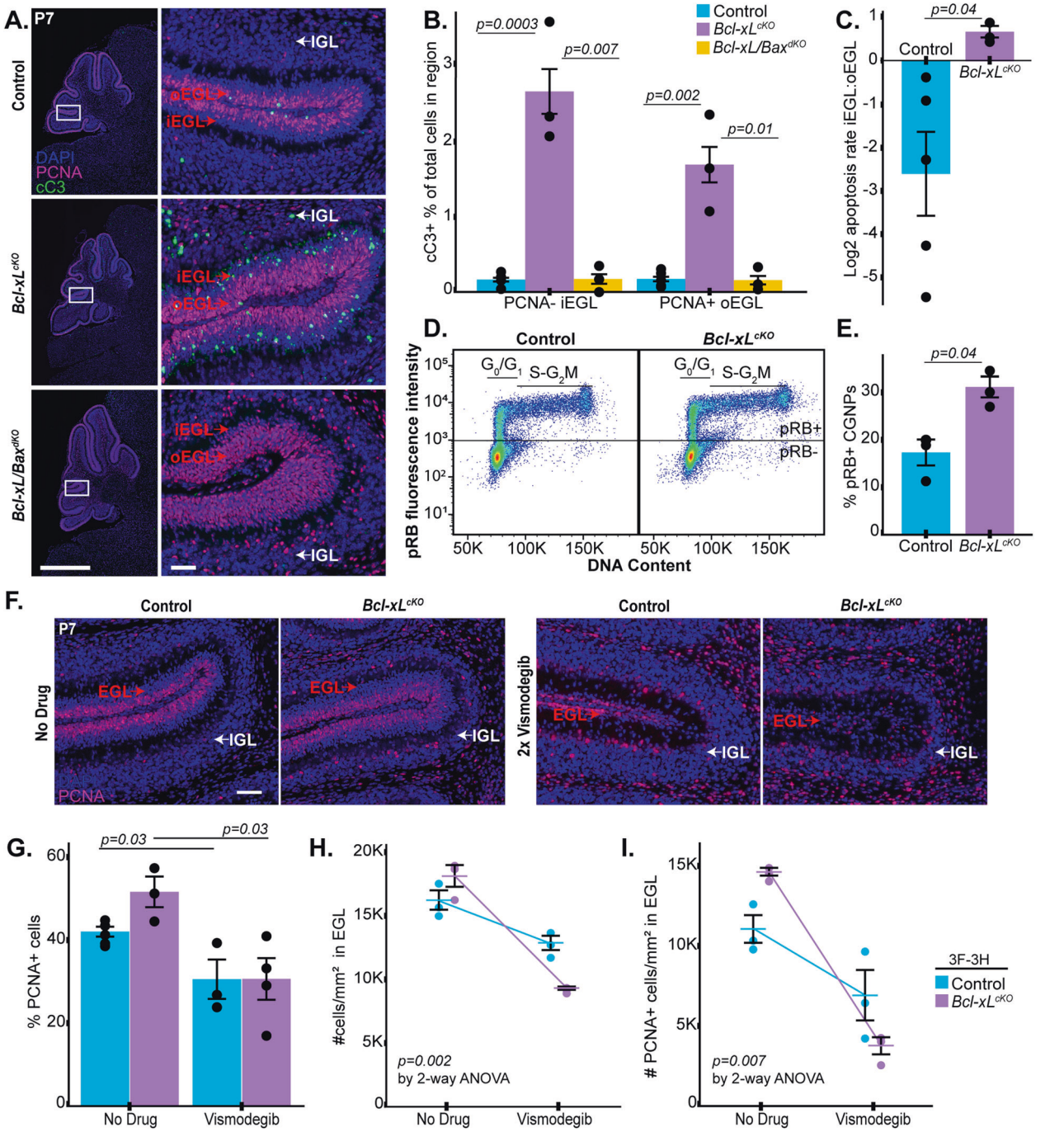

Fig. 3 Apoptosis in *Bcl-xL*^{cKO} CGNPs is linked to cell cycle exit. A–C Representative PCNA/cC3 IF in sagittal cerebellar sections from P7 *Bcl-xL*^{cKO}, *Bcl-xL;Bax*^{dKO}, and control mice, with **B** quantification of the %cC3^{+} cells in the PCNA^{+} oEGL and PCNA^{-} iEGL, and **C** log ratio of apoptotic rate iEGL:oEGL, for the indicated genotypes. **D, E** Representative flow cytometry studies of pRB versus DNA content in dissociated P7 CGNPs of the indicated genotypes, with the quantification of pRB^{+} cells showing significantly higher fraction of pRB+ cells in *Bcl-xL*^{cKO} mice. **F, G** Representative PCNA IF in sagittal cerebellar sections from P7 *Bcl-xL*^{cKO} and control mice treated with either vehicle or vismodegib at P5 and P6. Quantification of %PCNA^{+} cells in whole cerebellar sections from indicated genotypes and treatments shows that vismodegib reduces PCNA in both genotypes. Two-way ANOVA comparisons of EGL **(H)** total cell density and **(I)** density of PCNA^{+} cells show that vismodegib reduces total cell population and PCNA^{+} population more effectively in *Bcl*^{cKO} mice. Arrows indicate the IGL, EGL, oEGL, and iEGL regions. Size markers indicate 1 mm in low magnification images and 50 µm in high magnification images. All IF images are counterstained with DAPI. *P* values in **B**, **C**, **E**, and **G** determined by two-tailed Student's *t*-test. *P* values (**H**, **I**) determined by two-way ANOVA.

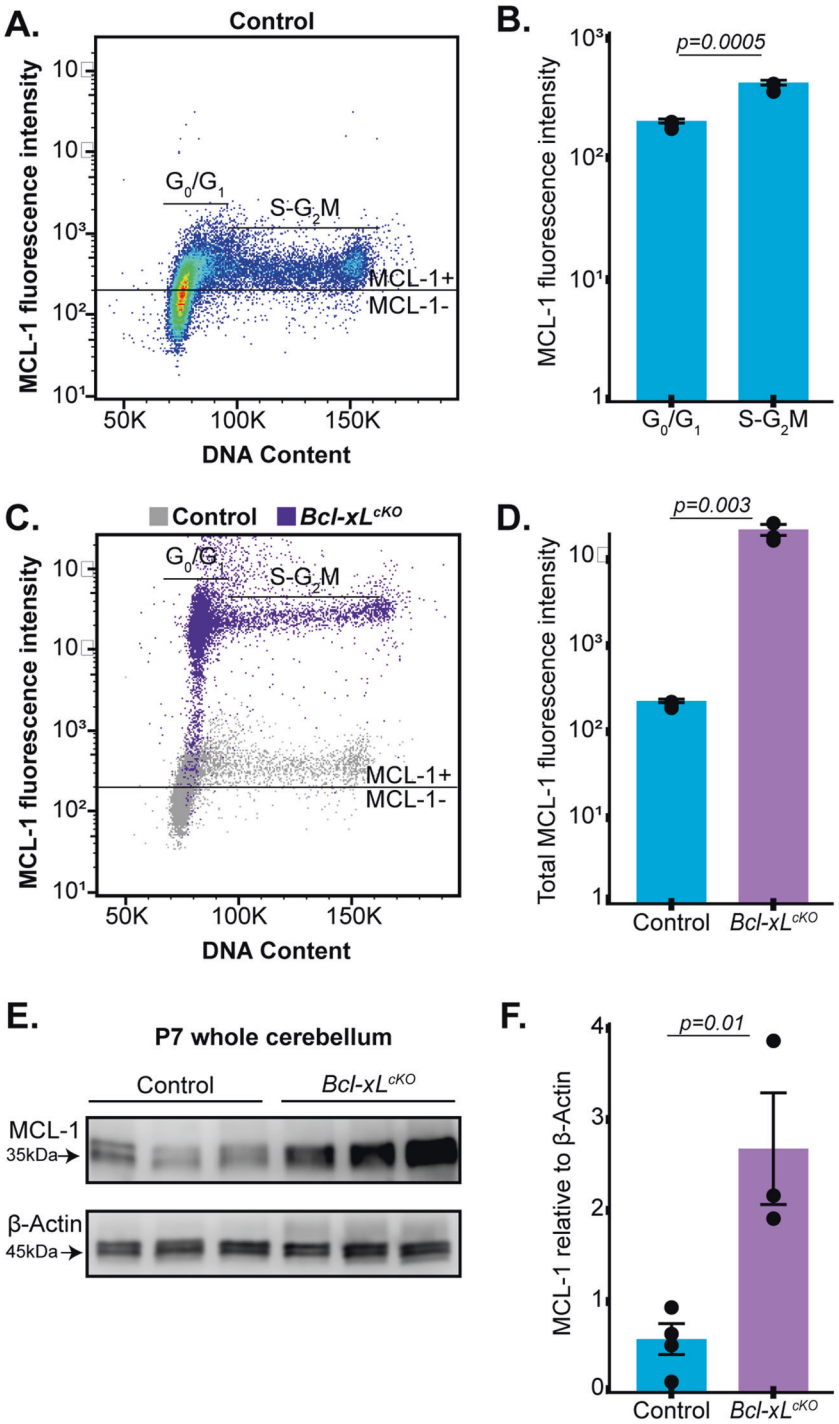

Fig. 4 MCL-1 is more abundant in proliferating CGNPs and is markedly increased in *Bcl-xL^{cKO}* mice. A, **B** Representative dot plots of MCL-1 IF versus DNA content, measured by flow cytometry and stratified into G_0/G_1, S, and G_2/M fractions, with the quantification of MCL-1 MFI in G_0/G_1, S -G_2/M phases. **C**, **D** Representative dot plots as in **A**, comparing MCL-1 in CGNPs of P7 *Bcl-xL^{cKO}* and control mice, with the quantification of MCL-1 MFI across all phases of the cell cycle in CGNPs from the indicated genotypes. **E**, **F** Representative western blots comparing the abundance of MCL-1 protein in lysates of whole cerebella of P7 *Bcl-xL^{cKO}* and control mice, with the quantification of MCL-1 abundance normalized to β-actin and expressed as fold change. Dot plots indicate data from individual replicate mice and horizontal bars with error bars indicate the mean ± SEM. *P* values determined by two-tailed Student's *t*-test.

CGNPs suggests a homeostatic mechanism in which MCL-1 stability increases in response to reduced BCL-xL. This homeostatic mechanism involved BAX protein, as MCL-1 was not increased in *Bcl-xL/Bax^{dKO}* cerebella (Supplementary Fig. 3), suggesting that the presence BAX not bound to BCL-xL alters MCL-1 degradation.

To determine if other key apoptosis regulators were increased in the *Bcl-xL^{cKO}* CGNPs, we examined the abundance of BCL-2 family members BAX and BCL-2, and the BH3-only proteins BIM and PUMA. Comparing *Bcl-xL^{cKO}* and control CGNPs, we found a statistically significant increase in BIM, while BAX, BCL-2 and PUMA remained similar between genotypes (Supplementary Fig. 2). As BIM is pro-apoptotic, this increase is not expected to inhibit cell death. The dramatic increase in MCL-1 was therefore only in antiapoptotic change that we detected in the apoptosis regulators.

MCL-1 compensates for BCL-xL in proliferating CGNPs

To test directly whether MCL-1 may compensate for BCL-xL, potentially maintaining the survival of proliferating CGNPs in *Bcl-xL*^{cKO} mice, we generated animals with co-deletion of *Mcl-1* and *Bcl2l1*. We accomplished this co-deletion by breeding *Bcl-xL*^{cKO} mice with *Mcl-1*$^{loxP/loxP}$ [16] mice to create the *Math1-Cre/Bcl2l1*$^{loxP/loxP}$;*Mcl-1*$^{loxP/loxP}$ (*Bcl-xL/Mcl-1*^{dKO}) genotype. As an intermediate in the course of this breeding, we also generated *Math1-Cre/Bcl2l1*$^{loxP/+}$/*Mcl-1*$^{loxP/loxP}$ mice that carried Math1-Cre and were heterozygous for *Bcl2l1* and homozygous for *Mcl-1* (*Bcl-xL*^{HET}/*Mcl-1*^{cKO}). *Bcl-xL*^{HET}/*Mcl-1*^{cKO} mice developed mild cerebellar hypoplasia (Fig. 5A) that was not symptomatic. This hypoplasia was in contrast to the normal appearing cerebella of both *Math1-Cre/Bcl2l1*$^{loxP/+}$ (*Bcl-xL*^{HET}) mice where *Bcl2l1* was heterozygous and *Mcl-1* was WT, and *Math1-Cre/Mcl-1*$^{loxP/\ loxP}$ (*Mcl-1*^{cKO}) *mice where Bcl2l1* was WT and *Mcl-1* was deleted (Fig. 5A). The phenotype of *Bcl-xL*^{HET}/*Mcl-1*^{cKO} show that *Bcl2l1* heterozygosity induced a requirement for MCL-1 that was not apparent when *Bcl2l1* was WT, and similarly, that *Mcl-1* deletion, induced a requirement for both copies of *Bcl2l1* to be intact. The intermediate *Bcl-xL*^{HET}/*Mcl-1*^{cKO} genotype thus provided initial evidence that BCL-xL and MCL-1 operate redundantly in CGNPs.

Homozygous conditional deletion of *Bcl2l1* and *Mcl-1* in *Bcl-xL/Mcl-1*^{dKO} mice produced more severe cerebellar growth failure than *Bcl-xL*^{HET}/*Mcl-1*^{cKO} mice. Like *Bcl-xL*^{cKO} mice, *Bcl-xL/Mcl-1*^{dKO} mice were ataxic but viable and fertile. However, growth failure began earlier than in *Bcl-xL*^{cKO} mice, as cerebella in *Bcl-xL/Mcl-1*^{dKO} mice showed markedly reduced size and foliation beginning as early as P7, with sparing of the posterior-inferior region producing a sharply contrasting region by P16 (Fig. 5B). Apoptosis was also distributed differently, localizing primarily to the EGL of *Bcl-xL/Mcl-1*^{dKO} cerebella and occurred primarily in proliferating, PCNA^{+} CGNPs (Fig. 5C, D). In *Bcl-xL/Mcl-1*^{dKO} cerebella, fewer CGNPs survived to cell cycle exit, resulting in failure to generate a distinguishable IGL (Fig. 5E). The enhanced growth failure and accelerated apoptosis compared to *Bcl-xL*^{cKO} mice, demonstrates that MCL-1 suppresses apoptosis in parallel with BCL-xL in the proliferating subset of CGNPs.

Bcl-xL^{cKO} CGNPs show increased SHH-driven proliferation, suggesting SUFU:MCL-1 interaction

MCL-1, BCL-xL, and BCL-2 have recently been reported to be positive regulators SHH signaling that act by inhibiting SUFU, which is a negative regulator of SHH [32]. In light of this report and our finding of dramatically increased MCL-1 protein in *Bcl-xL*^{cKO} CGNPs, we examined whether *Bcl-xL*^{cKO} CGNPs at P12 showed increased SHH activation compared to controls. Consistent with increased SHH activation, we found greater proportions of cells in the *Bcl-xL*^{cKO} EGL expressing SHH target genes MATH1 (aka ATOH-1), and CCND1 (Fig. 6A–D). A less marked increase in MATH1 and CCND1 was also noted in the posterior-inferior lobules where Bcl-xL deletion was mosaic. Importantly, vismodegib blocked CGNP hyperproliferation in P12 *Bcl-xL*^{cKO} mice, confirming that the observed hyperproliferation was driven by increased SHH signaling (Fig. 6E, F).

We used immunoprecipitation to determine if *Bcl-xL*^{cKO} CGNPs showed increased MCL-1:SUFU interaction that could mediate increased SHH activation. We immunoprecipitated MCL-1 under nondenaturing conditions in *Bcl-xL*^{cKO} and WT CGNP lysates. We then used western blot to compare MCL-1 and SUFU abundance. MCL-1 was enriched in *Bcl-xL*^{cKO} input lysates and immunoprecipiates, as expected. SUFU was not more abundant in P7 *Bcl-xL*^{cKO} cerebellum lysates (Supplementary Fig. 4), but SUFU was markedly increased in the *Bcl-xL*^{cKO} MCL-1 immunoprecipitates (Fig. 6G). As an alternative way to increase MCL-1 abundance in the presence of BCL-xL, we exposed WT CGNPs in vivo to ionizing radiation 3 h prior to harvest, which we found also increases MCL-1 abundance. Despite high MCL-1 in these radiated CGNPs, SUFU was not increased in the MCL-1 IP from irradiated cerebella. These studies show that in the specific condition of BCL-xL depletion, the MCL-1:SUFU interaction increases. We speculate that increased MCL-1 binding of SUFU increases SHH pathway activation downstream of the PTC-SMO receptor complex as previously described in other cell types [32], while simultaneously reducing MCL-1 degradation.

Discussion

Our data show that neural progenitors continuously require antiapoptotic BCL-xL to maintain their survival as they progress from proliferative undifferentiated cells to neurons. Conditional deletion of *Bcl2l1* in the *Math1* lineage in *Bcl-xL*^{cKO} mice prevented BCL-xL expression in CGNPs and caused symptomatic cerebellar growth failure. This growth failure was caused by spontaneous apoptosis that occurred sporadically, at an increased rate compared to BCL-xL-intact controls. Proliferative CGNPs of the oEGL, nonproliferative CGNPs of the iEGL and CGNs of the IGL all showed increased apoptotic frequency. BCL-xL dependency was higher in non-proliferating cells, including differentiating CGNPs and CGNs, than in proliferating CGNPs, causing the IGL to be disproportionately depleted.

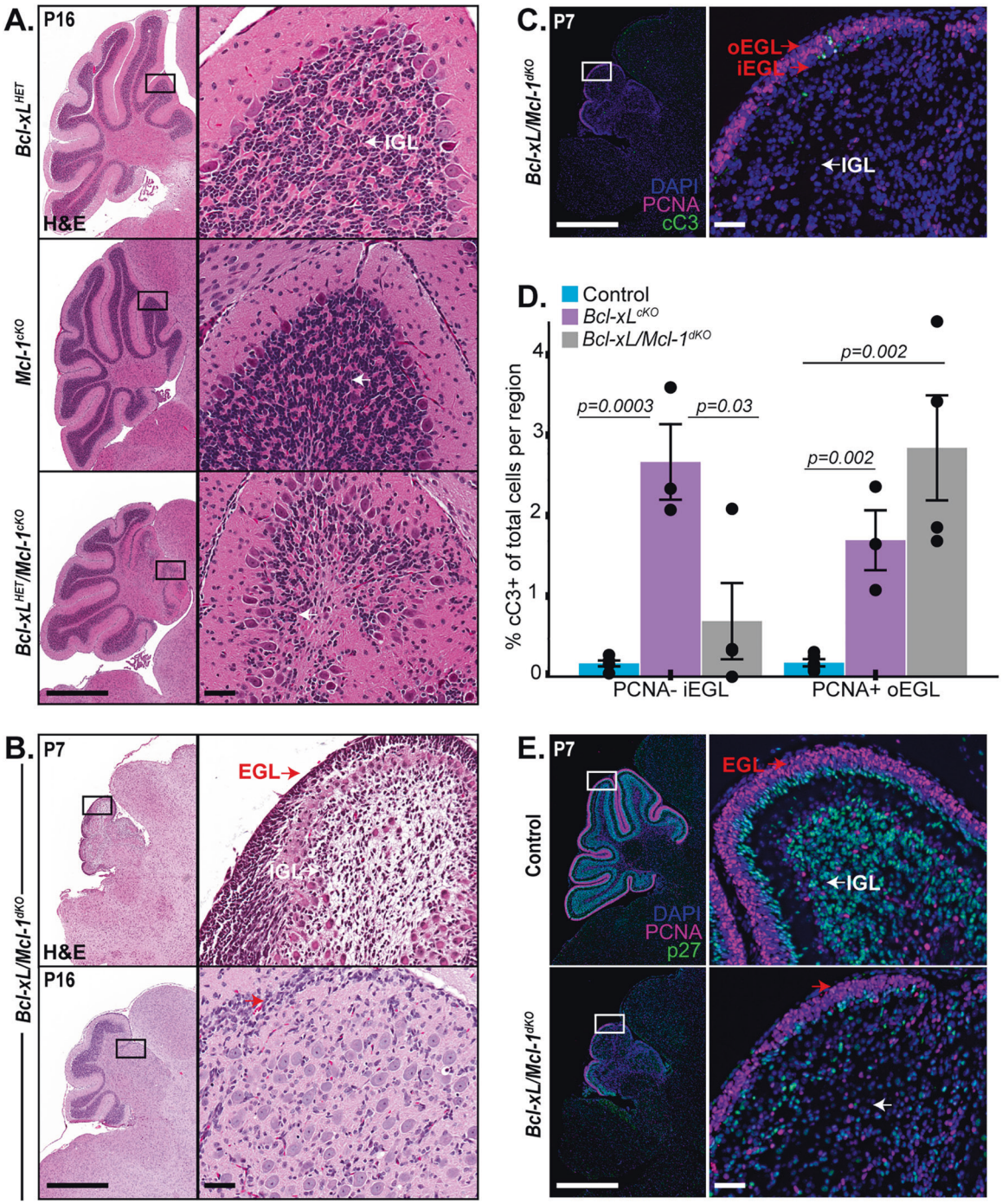

Fig. 5 MCL-1 compensates for BCL-xL in proliferating CGNPs. A Representative sagittal H&E-stained sections comparing of cerebella from P16 *Bcl-xl*^{HET}, and *MCL-1*^{cKO}, and *Bcl-xL*^{HET}/*Mcl-1*^{cKO} mice. **B** Representative sagittal H&E-stained section of a *Bcl-xL/Mcl-1*^{dKO} cerebellum at P7 and P16. **C**, **D** Representative PCNA/cC3 IF in sagittal cerebellar sections from P7 *Bcl-xL/Mcl-1*^{dKO}, with quantification of the %cC3^{+} cells in the PCNA^{+} oEGL and PCNA^{-} iEGL from the indicated genotypes, showing increased cell death in the oEGL of *Bcl-xL/Mcl-1*^{dKO} mice and reduced cell death in the iEGL. **E** Representative PCNA/p27 IF in sagittal sections of P7 *Bcl-xL/Mcl-1*^{dKO} and WT control cerebella. In **D**, *Bcl-xL*^{cKO} and control mice from figure 3B are presented for comparison. Size markers indicate 1 mm in low magnification images and 50 µm in high magnification images All IF images are counterstained with DAPI. *P* values determined by two-tailed Student's *t*-test.

In addition to increased cell death, we also noted an increased duration of CGNP proliferation. While most CGNPs typically exit the EGL by P12, in P12 *Bcl-xL*^{cKO} mice the EGL remained abnormally thick and populated with proliferative cells. This prolonged period of CGNP proliferation was also seen in prior studies of *Bax*-deleted

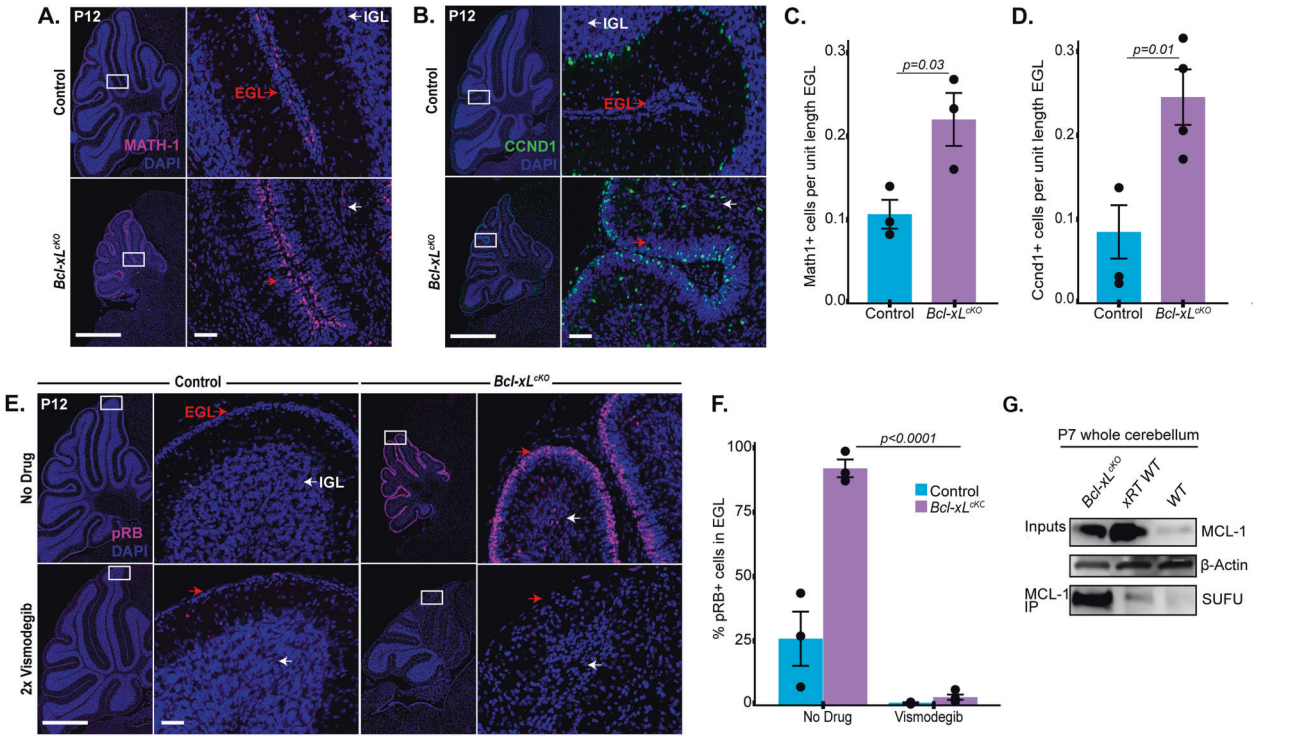

Fig. 6 Prolonged CGNP proliferation in P12 *Bcl-xL*^{cKO} mice is due to increased SHH activation. Representative **A** MATH1 and **B** CCND1 IF in sagittal cerebellar sections from P12 *Bcl-xL*^{cKO} and control mice, with the quantification of **C** MATH1^{+} cells or **D** CCND1^{+} cells per 200 µm length of EGL in the indicated genotypes. **E**, **F** Representative pRB IF in sagittal cerebellar sections from P12 *Bcl-xL*^{cKO} and control mice, with the quantification of %pRB+ cells in the EGL in the indicated genotypes. **G** IP study using MCL-1 antibodies, with western blots for indicated proteins on the input lysates or the immunoprecipitated protein (MCL-1 IP), as indicated. Microscopy size markers indicate 1 mm in low magnification images and 50 µm in high magnification images. All IF images are counterstained with DAPI. *P* values determined by two-tailed Student's *t*-test.

mice [18], and was abolished by co-deletion of *Bax* in *Bcl-xL/Bax*^{dKO} mice. The interaction of BCL-xL, BAX and proliferation suggests that imbalance of BCL-xL to BAX ratio in either direction is sufficient to alter proliferation, which is restored by co-deletion of both loci. The increased EGL thickness at P12 contrasts with the thinning of the IGL that is apparent at this time. Thus the two aspects of the phenotype of *Bcl-xL*^{cKO} mice were cerebellar hypoplasia that was apparent by P12 and was caused by excessive apoptosis, and persistent CGNP proliferation that ultimately waned by P15. Both of these aspects of the phenotype were BAX-dependent, as co-deletion of *Bax* in *Bcl-xL/Bax*^{dKO} rescued both growth failure and prolonged proliferation.

Our studies of MCL-1 demonstrated a mechanism for the relative preservation of proliferating CGNPs in *Bcl-xL*^{cKO} mice. We found that proliferating CGNPs in S-G_2/M phase consistently expressed MCL-1 protein while CGNPs in G_0-G_1 showed variable MCL-1 expression. BCL-xL depletion in the *Bcl-xL*^{cKO} mice further increased the abundance of MCL-1 protein in proliferating cells. The cell cycle-dependent expression of MCL-1 protein and the increased MCL-1 in BCL-xL-deficient CGNPs suggested that MCL-1 could be the mechanism preserving the survival of proliferating CGNPs in *Bcl-xL*^{cKO} mice. This role was confirmed by co-deletion of *Mcl-1* and *Bcl2l1* in *Bcl-xL/Mcl-1*^{dKO} mice, which increased spontaneous apoptosis in the proliferating CGNPs and enhanced the cerebellar growth failure phenotype. Taken together, our data show that CGNPs depend on BCL-xL to prevent spontaneous apoptosis, and that MCL-1 provides a redundant brake on apoptosis specifically during proliferation.

The increased expression of MCL-1 protein in CGNPs may also mediate the increased CGNP proliferation noted in P12 *Bcl-xL*^{cKO} mice. Both BCL-xL and MCL-1 have been shown to amplify SHH signaling by reducing the inhibitory effect of SUFU [32]. However, we found that MCL-1 abundance was linked to BCL-xL in CGNPs and increased 10-fold in the *Bcl-xL*^{cKO}. We speculate that this increase in MCL-1 amplified the developmentally waning SHH pathway activity in P12 *Bcl-xL*^{cKO} CGNPs. Consistent with increased SHH signaling, we noted that P12 *Bcl-xL*^{cKO} CGNPs showed increased expression of SHH targets MATH1 and CCND1. It was not possible to use genetic deletion to determine if MCL-1 mediated increased SHH signaling at P12, since proliferating CGNPs did not survive to P12 in *Bcl-xL/Mcl-1*^{dKO}. However, the coincidence of

increased MCL-1 and prolonged proliferation provides circumstantial evidence to support this mechanism. In light of these data, we propose that BCL-xL expression positively regulates CGNP differentiation by suppressing the abundance of MCL-1.

Our MCL-1 studies in CGNPs do not demonstrate the dependence seen in other models of *Mcl-1* deletion in different parts of the nervous system. We found that CGNPs with *Mcl-1* deletion were sensitized to *Bcl2l1* haploinsufficiency but otherwise showed normal survival and development, indicating that BCL-xL and MCL-1 act in concert, with BCL-xL as the primary brake on CGNP apoptosis. It remains possible that the requirement for *Mcl-1* is greater in progenitors outside of the Math1 lineage, as seen in prior studies of cortical and SVZ progenitors [11, 14]. However, our data make clear that MCL-1 is not required for all neural progenitors.

Overall, our data show that antiapoptotic BCL-2 proteins are required at all phases of neural progenitor maturation, but that the requirement for specific BCL-2 family proteins varies with proliferative state. Functional redundancy during proliferation reduces the dependence of proliferating progenitors on individual BCL-2 family members. MCL-1 is not required during CGNP development because BCL-xL can meet the requirement of both proliferating and differentiating progenitors. In contrast, proliferating CGNPs show relatively less BCL-xL dependence because MCL-1 can partially compensate for BCL-xL depletion. This compensation is facilitated by a homeostatic mechanism that increases MCL-1 abundance in BCL-xL-depleted cells. The potentiating effect of MCL-1 on mitogenic SHH signaling further increases the tendency of surviving cells to be proliferative. Conversely differentiating CGNPs, which have lower MCL-1, are most dependent on BCL-xL. Through these mechanisms, the proximity of CGNPs to the apoptotic threshold is modulated as CGNPs progress through development to CGNs, while antiapoptotic mechanisms provide regulatory feedback on the differentiation process.

Acknowledgements We thank the UNC Center for Gastrointestinal Biology and Disease Histology Core (supported by P30DK03987) for processing tissue sections and staining for H&E, Gabriela De la Cruz and Stephanie Cohen in the UNC Translational Pathology Laboratory (TPL) for help staining, digitizing, and quantifying sections. TPL is supported, in part, by grants from the NCI (P30CA016086-42), NIH (U54-CA156733), NIEHS (P30 ES010126-17), UCRF and NCBT (2015-IDG-1007). We also thank the UNC Flow Cytometry Core Facility for assistance. We thank David Rowitch (UCSF, San Francisco, CA) and Robert Wechsler-Reya (Sanford-Burnham Medical Research Institute, La Jolla, CA) for the *Math1-Cre* mice. Supported by NINDS F31NS101883, R01NS088219, R01NS102627, and R01NS1062, and NCI T32CA071341.

Funding KAV was supported by an F31 award from the NINDS (1F31NS101883). AC and TRG were supported by grants from the NINDS (R01NS088219, R01NS102627, R01NS106227) and the St. Baldrick's Foundation.

Compliance with ethical standards

Conflict of interest The authors declare that they have no conflict of interest.

Publisher's note Springer Nature remains neutral with regard to jurisdictional claims in published maps and institutional affiliations.

References

1. Kenney AM, Rowitch DH. Sonic hedgehog promotes G1 cyclin expression and sustained cell cycle progression in mammalian neuronal precursors. Mol Cell Biol. 2000;20:9055–67. https://doi.org/10.1128/mcb.20.23.9055-9067.2000.
2. Hatten ME, Heintz N. Mechanisms of neural patterning and specification in the development cerebellum. Ann Rev Neurosci. 1995;18:385–408. https://doi.org/10.1146/annurev.ne.18.030195.002125.
3. Roussel MF, Hatten ME. Cerebellum development and medulloblastoma. Curr Top Dev Biol. 2011;94:235–82. https://doi.org/10.1016/B978-0-12-380916-2.00008-5.
4. Crowther AJ, Gama V, Bevilacqua A, Chang SX, Yuan H, Deshmukh M, et al. Tonic activation of Bax primes neural progenitors for rapid apoptosis through a mechanism preserved in medulloblastoma. J Neurosci. 2013;33:18098–108. https://doi.org/10.1523/JNEUROSCI.2602-13.2013.
5. Dumitru R, Gama V, Fagan BM, Bower JJ, Swahari V, Pevny LH, et al. Human embryonic stem cells have constitutively active bax at the golgi and are primed to undergo rapid apoptosis. Mol Cell. 2012;46:573–83. https://doi.org/10.1016/j.molcel.2012.04.002.
6. Sarosiek KA, Fraser C, Muthalagu N, Bhola PD, Chang W, McBrayer SK, et al. Developmental regulation of mitochondrial apoptosis by c-Myc governs age- and tissue-specific sensitivity to cancer therapeutics. Cancer Cell. 2017;31:142–56. https://doi.org/10.1016/j.ccell.2016.11.011.
7. Deng J, Carlson N, Takeyama K, Dal Cin P, Shipp M, Letai A. BH3 profiling identifies three distinct classes of apoptotic blocks to predict response to ABT-737 and conventional chemotherapeutic agents. Cancer Cell. 2007;12:171–85. https://doi.org/10.1016/j.ccr.2007.07.001.
8. Ryan JA, Brunelle JK, Letai A. Heightened mitochondrial priming is the basis for apoptotic hypersensitivity of CD4+ CD8+ thymocytes. Proc Natl Acad Sci USA. 2010;107:12895–900. https://doi.org/10.1073/pnas.0914878107.
9. Nakamura A, Swahari V, Plestant C, Smith I, McCoy E, Smith S, et al. Bcl-xL is essential for the survival and function of differentiated neurons in the cortex that control complex behaviors. J Neurosci. 2016;36:5448–61. https://doi.org/10.1523/JNEUROSCI.4247-15.2016.
10. Harder JM, Ding Q, Fernandes KA, Cherry JD, Gan L, Libby RT. BCL2L1 (BCL-X) promotes survival of adult and developing retinal ganglion cells. Mol Cell Neurosci. 2012;51:53–9. https://doi.org/10.1016/j.mcn.2012.07.006.
11. Fogarty LC, Song B, Suppiah Y, Hasan SMM, Martin HC, Hogan SE, et al. Bcl-xL dependency coincides with the onset of neurogenesis in the developing mammalian spinal cord. Mol Cell Neurosci. 2016;77:34–46. https://doi.org/10.1016/j.mcn.2016.09.001.
12. Fogarty LC, Flemmer RT, Geizer BA, Licursi M, Karunanithy A, Opferman JT, et al. Mcl-1 and Bcl-xL are essential for survival of

the developing nervous system. Cell Death Differ. 2019;26: 1501–15. https://doi.org/10.1038/s41418-018-0225-1.
13. Arbour N, Vanderluit JL, Le Grand JN, Jahani-Asl A, Ruzhynsky VA, Cheung EC, et al. Mcl-1 is a key regulator of apoptosis during CNS development and after DNA damage. J Neurosi. 2008;28:6068–78. https://doi.org/10.1523/JNEUROSCI.4940-07.2008.
14. Malone CD, Hasan SM, Roome RB, Xiong J, Furlong M, Opferman JT, et al. Mcl-1 regulates the survival of adult neural precursor cells. Mol Cell Neurosci. 2012;49:439–47. https://doi.org/10.1016/j.mcn.2012.02.003.
15. Zhang N, He YW. The antiapoptotic protein Bcl-xL is dispensable for the development of effector and memory T lymphocytes. J Immunol. 2005;174:6967–73.
16. Dzhagalov I, St John A, He YW. The antiapoptotic protein Mcl-1 is essential for the survival of neutrophils but not macrophages. Blood. 2007;109:1620–6. https://doi.org/10.1182/blood-2006-03-013771.
17. Lang PY, Nanjangud GJ, Sokolsky-Papkov M, Shaw C, Hwang D, Parker JS, et al. ATR maintains chromosomal integrity during postnatal cerebellar neurogenesis and is required for medulloblastoma formation. Development. 2016;143:4038–52. https://doi.org/10.1242/dev.139022.
18. Garcia I, Crowther AJ, Gama V, Miller CR, Deshmukh M, Gershon TR. Bax deficiency prolongs cerebellar neurogenesis, accelerates medulloblastoma formation and paradoxically increases both malignancy and differentiation. Oncogene. 2013;32: 2304–14. https://doi.org/10.1038/onc.2012.248.
19. Luxenhofer R, Schulz A, Roques C, Li S, Bronich TK, Batrakova EV, et al. Doubly amphiphilic poly(2-oxazoline)s as high-capacity delivery systems for hydrophobic drugs. Biomaterials. 2010;31:4972–9. https://doi.org/10.1016/j.biomaterials.2010.02.057.
20. Wan X, Beaudoin JJ, Vinod N, Min Y, Makita N, Bludau H, et al. Co-delivery of paclitaxel and cisplatin in poly(2-oxazoline) polymeric micelles: Implications for drug loading, release, pharmacokinetics and outcome of ovarian and breast cancer treatments. Biomaterials. 2019;192:1–14. https://doi.org/10.1016/j.biomaterials.2018.10.032.
21. Hwang D, Dismuke T, Tikunov A, Rosen EP, Kagel JR, Ramsey JD, et al. Poly(2-oxazoline) nanoparticle delivery enhances the therapeutic potential of vismodegib for medulloblastoma by improving CNS pharmacokinetics and reducing systemic toxicity. https://www.biorxiv.org/content/10.1101/2020.04.30.068726v1. https://doi.org/10.1101/2020.04.30.068726.
22. Machold R, Fishell G. Math1 is expressed in temporally discrete pools of cerebellar rhombic-lip neural progenitors. Neuron. 2005;48:17–24. https://doi.org/10.1016/j.neuron.2005.08.028.
23. Matei V, Pauley S, Kaing S, Rowitch D, Beisel KW, Morris K, et al. Smaller inner ear sensory epithelia in Neurog1 null mice are related to earlier hair cell cycle exit. Developmental Dyn. 2005;234:633–50. https://doi.org/10.1002/dvdy.20551.
24. Helms AW, Abney AL, Ben-Arie N, Zoghbi HY, Johnson JE. Autoregulation and multiple enhancers control Math1 expression in the developing nervous system. Development. 2000;127: 1185–96.
25. Lorenz A, Deutschmann M, Ahlfeld J, Prix C, Koch A, Smits R, et al. Severe alterations of cerebellar cortical development after constitutive activation of Wnt signaling in granule neuron precursors. Mol Cell Biol. 2011;31:3326–38. https://doi.org/10.1128/MCB.05718-11.
26. Chow KH, Shin DM, Jenkins MH, Miller EE, Shih DJ, Choi S, et al. Epigenetic States of cells of origin and tumor evolution drive tumor-initiating cell phenotype and tumor heterogeneity. Cancer Res. 2014;74:4864–74. https://doi.org/10.1158/0008-5472.CAN-13-3293.
27. Von Hoff DD, LoRusso PM, Rudin CM, Reddy JC, Yauch RL, Tibes R, et al. Inhibition of the hedgehog pathway in advanced basal-cell carcinoma. N. Engl J Med. 2009;361:1164–72. https://doi.org/10.1056/NEJMoa0905360.
28. Hwang D, Zhao Y, Liu H, Kabanov A, Gershon T, Sokolsky M. MBRS-53. Enhanced efficacy of nano-formulated vismodegib shows the potential for polyoxazoline micelles to improve drug delivery to brain tumors. Neuro Oncol. 2018;20:i139–i40. https://doi.org/10.1093/neuonc/noy059.498.
29. Mojsa B, Lassot I, Desagher S. Mcl-1 ubiquitination: unique regulation of an essential survival protein. Cells. 2014;3:418–37. https://doi.org/10.3390/cells3020418.
30. Nijhawan D, Fang M, Traer E, Zhong Q, Gao W, Du F, et al. Elimination of Mcl-1 is required for the initiation of apoptosis following ultraviolet irradiation. Genes Dev. 2003;17:1475–86. https://doi.org/10.1101/gad.1093903.
31. Cuconati A, Mukherjee C, Perez D, White E. DNA damage response and MCL-1 destruction initiate apoptosis in adenovirus-infected cells. Genes Dev. 2003;17:2922–32. https://doi.org/10.1101/gad.1156903.
32. Wu X, Zhang LS, Toombs J, Kuo YC, Piazza JT, Tuladhar R, et al. Extra-mitochondrial prosurvival BCL-2 proteins regulate gene transcription by inhibiting the SUFU tumour suppressor. Nat Cell Biol. 2017;19:1226–36. https://doi.org/10.1038/ncb3616.